Test of a Conduction-Cooled, Prototype, Superconducting Magnet for a Compact Cyclotron

Philip C. Michael, Timothy A. Antaya, Alexi Radovinsky, Bradford A. Smith, and Shahin Pourrahimi

***Abstract*—A 208-mm inner diameter, 62-mm-tall, wind-and-react Nb_3Sn prototype magnet was tested to demonstrate its suitability for use in a compact superconducting cyclotron. The magnet and its 270 kg iron return yoke were cooled together by conduction using a 2-stage Gifford–McMahon cycle refrigerator. This paper presents thermal, electrical and electromagnetic data collected during the tests. Although the radiation shield for the assembly cooled to 47 K within one day, a total of nine days were needed to cool the magnet assembly to below 4 K, at an ultimate heat load of 0.2 W. The dominant heat load at each stage of the cold head was due to thermal conduction along the current leads. The coil was charged without quench to 211 A, generating a pole tip magnetic induction of 3 T. The test demonstrates the technical feasibility to design, manufacture and operate compact superconducting cyclotron magnets at currents in excess of 200 A. The results are being used to improve the design for future high-field, conduction-cooled superconducting cyclotrons.**

***Index Terms*—Conduction-cooled Nb_3Sn magnet, cryocooler, HTS current leads, superconducting cyclotron.**

I. Introduction

COMPACT superconducting cyclotrons are increasingly used for cancer treatment, nuclear medicine, ion implantation, nuclear materials testing, and national security [1]–[6]. The use of superconductivity can reduce the mass of a cyclotron by more than an order of magnitude, with significant reduction in overall cost [1]. During the past several years we have designed compact superconducting cyclotrons for most of the applications listed above. A few of these designs have been commercialized, while others remain under development as laboratory-based systems.

The tests in this paper were performed to assess a wide range of practical design options. The intent was not to examine a particular configuration but to examine design parameters which could be applied to a final cyclotron design. The test apparatus for this study was quickly assembled using equipment on hand, or readily obtainable.

One goal of the test was to demonstrate a magnet system using a wind-and-react Nb_3Sn coil in an aluminum housing. The housing facilitates mechanical handling, applies modest preload to the strain-sensitive conductor during cooling, reacts Lorentz loads, and helps conduct heat from the coil. The development of robust and easy to produce Nb_3Sn coils allows us to evaluate cyclotron designs based on 10 K cryocoolers, which are typically lighter and less expensive to buy and operate than equivalent 4 K cryocoolers. The use of Nb_3Sn can also significantly increases the stability margin for higher field (> 6 T) cyclotrons operating near 4 K.

Manuscript received October 4, 2012; accepted November 30, 2012. Date of publication December 11, 2012; date of current version January 13, 2013. This work was supported in part by a Frontiers in Science grant of the Defense Threat Reduction Agency HDTRA-09-1-00042.

P. C. Michael, A. Radovinsky, and B. A. Smith are with the MIT Plasma Science and Fusion Center, Cambridge, MA 02139 USA (e-mail: michael@psfc.mit.edu; radovinsky@psfc.mit.edu; smith@psfc.mit.edu).

T. A. Antaya is with Ionetix Corporation, Hampton, NH 03842 USA (e-mail: tantaya@ionetix.com).

S. Pourrahimi is with Superconducting Systems, Inc., Billerica, MA 01821 USA (e-mail: pourrahimi@superconductingsystems.com).

Digital Object Identifier 10.1109/TASC.2012.2233539

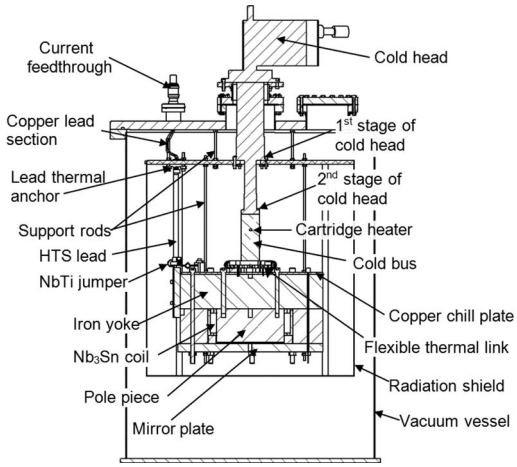

Fig. 1. Cross-section view of the test apparatus.

II. Test Apparatus

Fig. 1 shows a cross section view of the prototype magnet suspended within a 0.76 m diameter, 1 m tall vacuum chamber. The apparatus features a single Nb_3Sn coil in aluminum housing, surrounded by an ASTM A-36 steel yoke. At low beam energy (< 40 MeV) significant reduction in complexity can be achieved by incorporating the iron yoke into the cold mass. A mirror plate is used to close the yoke instead of using a second, symmetrically arranged coil and pole piece, as in a true cyclotron. The outer surface of the yoke is covered with 3 M series 425 aluminum tape to minimize radiant heat transfer to the cold mass [7]. Table I summarizes pertinent dimensions for the magnet assembly.

The magnet is surrounded by a thermal radiation shield and suspended using a set of three 1/4-20 threaded rods from the radiation shield's 12.7 mm thick, OFHC-copper top plate. The radiation shield, with 1.5 mm thick side walls, is similarly suspended from the top plate of the vacuum vessel and blanketed with 25 layers of 6.4 μm thick double-aluminized-mylar film procured from Rol-Vac LP of Dayville, CT.

The radiation shield and magnet are respectively cooled by attachment to the 1st and 2nd stages of a reconditioned Leybold

TABLE I
MAGNET PARAMETERS

Conductor type	Internal-tin strand
Conductor diameter	0.813 mm
Copper to non-copper ratio	1.38:1
Conductor insulation	S-2 glass
Diameter over conductor insulation	0.962 mm
Inner diameter of Nb_3Sn winding	208.5 mm
Outer diameter of Nb_3Sn winding	245.7 mm
Height of Nb_3Sn winding	61.6 mm
Number of layers in winding	22
Numbers of turns per layer	63
Iron yoke material	A36 steel
Outer diameter of iron yoke	444.5 mm
Height of iron yoke	237.5 mm
Mass of iron yoke	270 kg

RDK-408D2, 4 K cryocooler. The radiation shield top plate is rigidly attached to the 1st stage through a thin layer of Apiezon type-N thermal conductive grease, while the magnet is attached to the 2nd stage using a flexible link fabricated from copper braid. A 6.3 mm thick copper chill plate, affixed to the top surface of the yoke, helps to maintain a uniform temperature distribution across the yoke. A stand-alone test was performed to recharacterize the thermal performance of the cryocooler before it was installed in the test apparatus.

A 55.9 mm diameter, 144 mm long OFHC copper bus was installed at the 2nd stage of the cryocooler. It provides clearance for installation of 300 mm long HTS lead sections and is equipped with a 6.3 mm diameter, 38 mm long resistive cartridge heater part way along its length to permit elevated temperature operation of the magnet, for instance to simulate cooling using a two-stage, 10 K cryocooler.

A. Nb_3Sn Coil

The coil was wound using 0.813 mm Nb_3Sn strand from the ITER CS Model Coil program [8]. The strand was insulated with S-2 glass braid to a diameter of 0.962 mm by Supercon, Inc. of Shrewsbury, MA. The coil was wound and reacted at Superconducting Systems, Inc. in Billerica, MA. After reaction, three 30 mm lengths of 0.75 mm NbTi super-conductor were soldered to the coil leads to facilitate attachment to the test apparatus. The coil, with lead extensions, was then encased in an aluminum housing and vacuum pressure impregnated using CTD 512 epoxy. The total copper area in the lead extensions is roughly three times that of the Nb_3Sn stand.

Fig. 2 shows projected performance limits for the coil. The peak field load line was determined using Vector Fields Opera [9], while the critical current traces were estimated using quality assurance data and previously determined scaling relations [10]. The estimated strain in the Nb_3Sn following reaction is -0.25%, while that following cooldown is -0.4%.

B. Current Leads

The test apparatus is equipped with multi-section current leads. Most of the joints between sections are clamped to facilitate rapid reuse of components. Each copper lead section contains a vacuum feedthrough with 19 mm copper electrode and a pair of 4.62 mm (6 AWG) by 158 mm long copper magnet wires that are bent in zig-zag fashion to accommodate

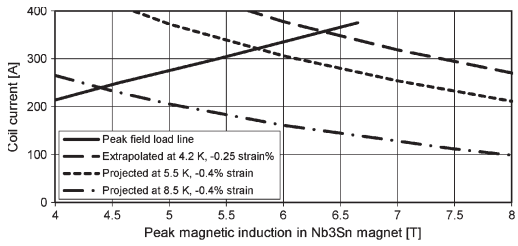

Fig. 2. Projected coil performance.

differential thermal contraction. The copper leads are optimized for operation at 600 A following design rules proposed by McFee [11]. The terminal blocks affixed to the feedthroughs outside the vacuum vessel are equipped with thermostatically controlled heaters to prevent icing in the absence of transport current.

The lower ends of the magnet wire extensions are soldered into 57 mm long by 13 mm wide copper blocks. These blocks are rigidly clamped to the lower surface of the radiation shield plate with a 50.8 μm Kapton sheet, coated on each side with Apiezon grease in the interface. Each block provides both a thermal anchor, to transfer heat conducted down and generated within the copper leads to the cryocooler 1st stage, and an electrical connection to a HTS lead section.

The HTS sections are 500 A rated Cryosaver leads, manufactured by HTS-110 Ltd. To facilitate differential thermal contraction, a 13 mm diameter half loop was formed into the NbTi jumpers before they were clamped to the HTS leads. Flex link assemblies were also used to intercept any heat conducted along or generated in the HTS leads, using Apiezon coated 50.8 μm Kapton sheet for electrical insulation at the clamped connection to the magnet chill plate.

C. Instrumentation

The temperatures of components attached to the cryocooler 1st stage were monitored using four Lakeshore type DT-670 silicon diodes. Silicon diodes were mounted to: the top of the 1st stage, bottom of the radiation shield, and at the upper ends of the HTS leads. The temperatures of components attached to the cryocooler 2nd stage were monitored using five Lakeshore type CX-150-AA Cernox sensors. Cernox sensors were mounted to: the top of the 2nd stage, top of the chill plate, lower ends of the HTS leads, and to an aluminum support ring inside the yoke assembly, beneath the coil.

A cable, containing eight voltage taps all twisted together, was used to monitor the lead section and coil terminal voltages. For each lead, voltage taps were attached to: the feed through electrode, the upper and lower end of the HTS leads, and the NbTi jumper as it enters the yoke. The voltage taps were grouped into twisted pairs at the air-side instrument feedthrough connector. Magnetic induction at the pole tip was monitored using a F.W. Bell BHT-921 Hall sensor. Lakeshore type QT-36 wiring was used for all in-vessel instruments.

D. Charging Circuit and Quench Protection

The configuration of the charging circuit, shown in Fig. 3, was dictated by quench protection concerns. Preliminary analysis using in-house quench codes showed that the coil must be

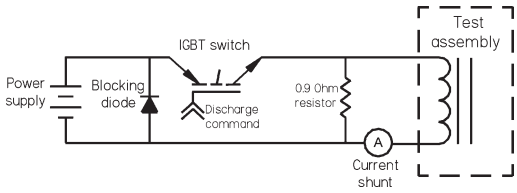

Fig. 3. Charging circuit schematic.

actively protected. The chief constraint was to limit the peak voltage during protection discharge to the 200 V in-vacuum ac voltage rating for our instrumentation feedthroughs. More general constraints were also applied, such as quench detection at the 50 mV level with 20 ms hold time and hot spot temperature below 150 K. Simulations indicated that these conditions could be met by limiting the coil current to below roughly 220 A, with current discharge through a 0.9 Ohm resistor.

Current was provided by a PowerTen 10 V, 1000 A supply which was connected through an IGBT switch, with 200 ns opening time, to one of the current feedthroughs. A lab built dump resistor, fabricated from a 12 m length of 12.7 mm wide by 0.76 mm thick stainless steel tape, was connected in parallel with the coil terminals. Current was measured using a calibrated, 500 A Crompton Instruments dc shunt in the return current leg. A 6 V diode, installed across the power supply terminals, protected it from switching transients. Not shown in Fig. 3 is the programmable logic controller that controlled the power supply, monitored the coil voltage, and if necessary opened the IGBT switch to discharge the coil current.

The coil was charged, using a series of trapezoidal ramps, to progressively higher current. Results in this paper come from a successful ramp to and from 211 A. During the next ramp, a quench at 236 A was detected. The protection circuit functioned as designed and the coil current discharged within 1 s of quench detection. The peak voltage during the dump was significantly less than anticipated, indicating significant internal resistance in the coil. Attempts to recharge the coil after recooling were unsuccessful. Examination of the coil after warm-up revealed two small sections of vaporized conductor near the top of the winding. The source of damage is not clear. It might have been caused by a small tin leak which locally poisoned the strand matrix during reaction [12], or perhaps the peak voltage during the current dump triggered sustained arcing at small defects in the strand insulation.

III. Experimental Results

A. Thermal Performance

Table II summarizes measured temperatures following cooldown and with the magnet energized to 211 A. During the first day of cooling the temperature at the 1st stage of the cryocooler decreased from room temperature to 46 K. Cooldown of the magnet cold mass took close to nine days, with a final temperature at the 2nd stage of 3.15 K. Raising the magnet current to a steady 211 A value increased the 1st stage temperature to 50 K and that at the 2nd stage to 3.45 K. Although we did not have many chances to use the cold bus heater during these experiments, preliminary tests showed that a heater power of 1.85 W would stably increase cold mass temperature from 3.5 K to 6.5 $\pm$ 0.2 K within an hour.

TABLE II
Measured Temperature Distribution

Location	Following cool-down	Energized at 211A
1st stage of cold head	46 K	50 K
Bottom or radiation shield	47 K	52 K
Upper end, left HTS lead	73 K	*
Upper end, right HTS lead	75 K	*
2nd stage of cold head	3.15 K	3.45 K
Copper chill plate	3.52 K	4.05 K
Lower end, left HTS lead	4.61 K	5.86 K
Lower end, right HTS lead	4.68 K	6.01 K

* Temperature readings on these sensors jumped to unrealistically high values when the power supply was connected to the test apparatus, even in the absence of output current.

TABLE III
Heat Loads on the Cold Head

Source	Following cool-down	Energized at 211A
1st stage heat loads		
Copper current leads	31.1 W	35.5 W
Gravity supports	1.4 W	1.4 W
Instrument lead wires	0.04 W	0.04 W
Radiation	4.3 W	4.3 W
Total	**36.9 W**	**41.3 W**
2nd stage heat loads		
HTS current leads, including joints	0.17 W	0.35 W
Gravity supports	0.01 W	0.01 W
Instrument lead wires	0.02 W	0.02 W
Radiation	<0.01 W	<0.01 W
Total	**0.20 W**	**0.38 W**

The projected temperature difference between the tops of the HTS leads and 1st stage was 10 K, whereas the measured difference was nearly three times higher. Our projection accounted for the 0.12 $\mathrm{W \cdot m^{-1} \cdot K^{-1}}$ thermal conductivity of Kapton [13] but overlooked the roughly 5000 $\mathrm{W \cdot m^{-2} \cdot K^{-1}}$ surface contact conductance through the Apiezon layer to the neighboring copper surfaces [14]. The right and left upper HTS lead temperatures following cooldown were 73 K and 75 K. Once the power supply was connected, their temperature could not be accurately measured due to ac pickup, which we could not entirely eliminate during these experiments [15].

Table III summarizes the evaluated heat loads on each stage of the cryocooler, both at zero current and with the coil energized to 211 A. Total heat loads were determined using our cryocooler calibration curve. Thermal conduction along the copper current leads, instrument wires, and gravity supports was determined from the component dimensions, high and low end temperatures, and thermal conductivity data from [16]–[18]. Thermal conduction along the HTS leads was estimated by linearly scaling the manufacturer's data to match our slightly higher high end temperatures [19]. The 1st stage radiation heat loads were estimated from calorimetric measurements on a similar cryostat in our lab [20], while those at the 2nd stage used rescaled data from [7] to match our much cooler radiation shield temperatures.

The 4.4 W increase in 1st stage heat load at 211 A is consistent with the electrically measured power dissipation in the copper leads; we observed 10.6 mV drop in the left lead and 10.2 mV in the right. The 0.18 W increase in 2nd stage heat load is largely due to heating at the clamped joints to the HTS leads. This heat load could be significantly reduced in a real device by soldering these joints instead.

TABLE IV
COMPUTED AND MEASURED MAGNETIC PERFORMANCE

Coil current [A]	Computed stored energy [J]	Computed magnetic induction [T]	Measured magnetic induction [T]
1	10	0.35	0.12
4	109	0.99	0.95
5	139	1.05	1.06
10	280	1.20	1.24
25	577	1.40	1.45
50	1328	1.75	1.77
75	2501	2.02	2.06
100	4090	2.22	2.27
150	8442	2.51	2.57
200	14267	2.78	2.85
211	15706	2.83	2.91

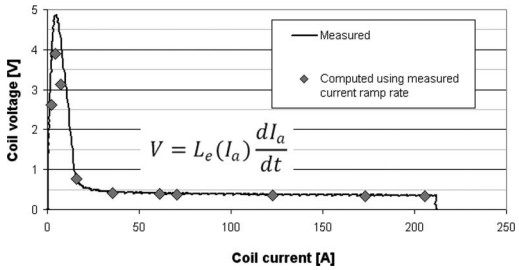

Fig. 4. Voltage across coil terminals versus current.

B. Electromagnetic Performance

Table IV summarizes the computed and measured magnetic performance for the prototype magnet. The computed results are from our Vector Fields Opera model. Measured and computed magnetic induction at the pole tip are consistent to within $\pm 3\%$, which is within the Hall probe's calibration accuracy at 4 K [21], except at low currents where resolution is reduced due to low signal levels.

Fig. 4 plots the measured and computed voltage across the coil terminals against coil current during a 0.5 $\mathrm{A \cdot s^{-1}}$ current ramp to 211 A. Agreement is quite good. Because of the iron yoke, the effective inductance of the coil, $L_e(I)$, varies markedly with coil current.

$$L_e(I_a) = \frac{2(E_2 - E_1)}{(I_2^2 - I_1^2)}, \quad \text{where} \quad I_a = \sqrt{I_1 I_2}. \qquad (1)$$

$L_e(I_a)$ is based on the computed data in Table IV, where E_2 and E_1 respectively are the stored magnetic energies at coil currents I_2 and I_1, and I_a is the average current at which the inductance is calculated.

IV. CONCLUSION

A test apparatus was assembled to examine design options relevant to compact, conduction-cooled superconducting cyclotrons. Our results show that it is feasible to conduction cool a superconducting magnet, including 270 kg iron yoke, to below 4 K at a static heat load below 0.25 W. We found that the cryogenic heat loads on the system are dominated by the current leads. Operation at currents up to 500 A is possible but requires significant improvement to our thermal anchor design, most likely through the use of finger joints with parallel cooling paths through the Kapton insulation. Although we are pleased with the coil results obtained thus far, we will continue to work on methods to improve performance and enhance the reliability of compact, conduction-cooled, Nb_3Sn-based magnets for cyclotron applications.

ACKNOWLEDGMENT

The authors thank D. Merdes, M. Zugger, E. Little, and D. Wess of the Applied Research Laboratory at the Pennsylvania State University for their support and assistance during the preparation and performance of these tests. We thank T. Bistany, presently at the Ionetics Corporation, for designing and procuring major components for the test apparatus and R. Lations of MIT-PSFC for assembling these components into a workable system.

REFERENCES

[1] S. Peggs, T. Satogawa, and J. Flanz, "A survey of hadron therapy accelerator technologies," in *Proc. IEEE Particle Accel. Conf.*, 2007, pp. 115–119.
[2] J. N. A. Matthews, "Accelerators shrink to meet growing demand for proton therapy," *Phys. Today*, vol. 62, no. 3, pp. 22–24, Mar. 2009.
[3] D. L. Friesel and T. A. Antaya, "Medical cyclotrons," in *Reviews of Accelerator Science and Technology*, vol. 2, A. W. Chao and W. Chou, Eds. NJ: World Scientific, 2009, pp. 133–156.
[4] D. M. Lewis, *Medical-Isotope Cyclotron Designs Go Full Circle*: CERN Courier, Apr. 2012.
[5] G. M. Wright, H. S. Barnard, Z. S. Hartwig, P. W. Stahle, R. M. Sullivan, K. B. Woller, and D. G. Whyte, "Plasma-surface interaction research at the Cambridge Laboratory of Accelerator Studies of Surfaces," in *Proc. 21st AIP Conf.—Appl. Accel. Res. Ind.*, 2011, pp. 626–630.
[6] R. C. Lanza and T. A. Antaya, "High energy protons for remote standoff detection of special nuclear materials," in *Proc. 11th Int. Conf. Appl. Nucl. Tech.*, 2011, pp. 153–160.
[7] A. F. Zeller, J. C. DeKamp, E. M. W. Leung, and R. W. Fast, "Long term results from the elimination of MLI between 4 and 77 K," *Adv. Cryo. Eng.*, vol. 39, pp. 1691–1697, 1994.
[8] R. Jayakumar, D. Gwinn, B. Montgomery, J. Minervini, C. Y. Gung, R. Randall *et al.*, "Fabrication of ITER central solenoid model coil inner module," *IEEE Trans. Appl. Supercond.*, vol. 7, pp. 981–984, Jun. 1997.
[9] Vector Fields Opera Software. [Online]. Available: http://www.cobham.com/technicalservices
[10] L. F. Goodrich, N. Cheggour, J. W. Ekin, and T. C. Stauffer, "Critical-current measurements on ITER Nb_3Sn strands: Effect of temperature," *IEEE Trans. Appl. Supercond.*, vol. 17, pp. 1398–1401, Jun. 2007.
[11] R. McFee, "Optimum input leads for cryogenic apparatus," *Rev. Sci. Instrum.*, vol. 20, pp. 98–102, Feb. 1959.
[12] P. J. Lee and D. C. Larbalestier, "Microstructural factors important for the development of high critical current density Nb_3Sn strands," *Cryogenics*, vol. 48, pp. 283–292, Aug. 2008.
[13] *Material Properties: Polyimide (Kapton)*, Nat. Inst. Stand. Technol., Boulder, CO. [Online]. Available: http://cryogenics.nist.gov/MPropsMAY/Polyimide%20Kapton/PolyimideKapton_rev.htm
[14] E. Gmelin, M. Asen-Palmer, M. Reuther, and R. Villar, "Thermal boundary resistance of mechanical contacts between solids at sub-ambient temperatures," *J. Phys. D, Appl. Phys.*, vol. 32, pp. R19–R43, 1999.
[15] J. K. Krause and B. C. Dorill, "Measurement system induced errors in diode thermometry," *Rev. Sci. Instrum.*, vol. 57, pp. 661–665, Apr. 1986.
[16] *Material Properties: OFHC Copper (UNS C10100/C10200)*, Nat. Inst. Stand. Technol., Boulder, CO. [Online]. Available: http://cryogenics.nist.gov/MPropsMAY/OFHC%20Copper/OFHC_Copper_rev.htm
[17] *Cryogenic Accessories: Wire*, Lake Shore Cryotronics, Inc., Westerville, OH. [Online]. Available: http://lakeshore.com/Documents/LSTC_wire_l.pdf
[18] *Material Properties: 304 Stainless (UNS S30400)*, Nat. Inst. Stand. Technol., Boulder, CO. [Online]. Available: http://cryogenics.nist.gov/MPropsMAY/304Stainless/304Stainless_rev.htm
[19] *HTS-110 Current Leads Brochure*, HTS-110, Ltd., Lower Hutt, New Zealand. [Online]. Available: http://www.hts110.co.nz/downloads/current-leads/HTS-110-current-leads.pdf
[20] P. C. Michael, J. H. Schultz, B. A. Smith, P. H. Titus, A. Radovinsky, A. Zhukovsky *et al.*, "Performance of the conduction-cooled LDX levitation coil," *Adv. Cryog. Eng.*, vol. 49A, pp. 701–710, 2005.
[21] F. W. Bell, Bulk Indium BH-900 Series Hall Sensors. [Online]. Available: http://fwbell.com/file/BH900.pdf